A non-linear model for the atomization of a swirling viscous liquid jet

E A Ibrahim* and **T L Williams**
Mechanical Engineering Department, Tuskegee University, Tuskegee, Alabama, USA

The manuscript was received on 25 July 2007 and was accepted after revision for publication on 14 May 2008.

DOI: 10.1243/09544062JMES810

Abstract: The instability and consequent atomization of a swirling viscous liquid jet emanated into gaseous surroundings and subjected to periodical surface disturbances is modelled and investigated. The theoretical analysis is based on a simplified mathematical formulation of the continuity and momentum equations in their conservative forms. Numerical solutions of the governing equations along with appropriate initial and boundary conditions are obtained through a robust finite-difference scheme. The computations yield real-time evolution of the interfacial profile and subsequent breakup characteristics of the liquid jet. It is found that the jet disintegrates into main and satellite drops, under all the conditions considered in the present study. The swirl enhances the instability of the jet and causes radial stretching of the main drops, whereas the satellite drops exhibit axial elongation. Increasing viscosity hinders jet instability and leads to main and satellite drop deformations that are similar to those produced by the swirl. The sizes of both main and satellite drops are diminished at higher disturbance wave numbers. A greater swirl strength induces a higher dominant wave number, and hence a reduced size of resultant main and satellite drops. Larger satellite drops and smaller main drops are produced as viscous forces are increased. The present model could be used as a guide for designing swirl injectors.

Keywords: non-linear, instability, atomization, swirl, liquid jet

1 INTRODUCTION

The instability and breakup of a liquid jet into small drops have a wide array of industrial applications including fuel injection, ink-jet printing, and spray delivery devices used for agricultural, medical, hygienic, coating, drying, and painting purposes. Therefore, numerous investigations have contributed to advancing models aimed at predicting the characteristics of the spray produced by liquid jet disintegration. These characteristics include breakup length and time, spray angle, drop size, velocity, and orientation.

Many of the existing models of jet atomization are linearized [**1**–**10**] and, hence, incapable of providing accurate predictions of resultant spray parameters because atomization is a highly non-linear phenomenon. Other models [**11**–**13**] were riddled with empiricism, which limit their applications to the range of experimental data employed in deriving their empirical formulae. Therefore, it is imperative to advance a jet atomization model that accounts for non-linear effects and is free of empirical relations.

Early attempts at formulating non-linear models of liquid jet atomization have exploited varied analytical approaches. Wang [**14**], Yuen [**15**], Nayfeh [**16**] and Nayfeh and Hassan [**17**], Kakutani *et al.* [**18**], Lafrance [**19**], Taub [**20**], and Chaudhary and Redekopp [**21**] used the method of strained coordinates. Bogy [**22**–**26**] employed the Cosserat theory developed by Green [**27**, **28**]. A weakly non-linear instability analysis was advanced by Ibrahim and Lin [**29**]. More recent modelling efforts utilized a multitude of numerical techniques. Direct numerical solutions of Navier–Stokes equations in their axisymmetric form were obtained by Fromm [**30**] and Shokoohi and Elrod [**31**] for the viscous jet. Mansour and Lundgren [**32**] pioneered the application of the boundary-element method of jet atomization studies. Chacha *et al.* [**33**] applied the finite-difference method to the

*Corresponding author: Mechanical Engineering Department, Tuskegee University, Tuskegee, Alabama 36088, USA. email: emeei@tuskegee.edu

Downloaded from pic.sagepub.com at PENNSYLVANIA STATE UNIV on September 17, 2016

vorticity-stream function formulation of the Navier–Stokes equations in their treatment of the problem of instability and breakup of a liquid capillary column in a bounded immiscible phase. References [**7**], [**8**], [**11**] to [**13**], [**20**], [**33**], and [**34**] provide reviews of some experimental results of liquid jet atomization studies.

Lee [**35**], and later Pimbley and Lee [**36**], developed a one-dimensional non-linear-direct-simulation technique that proved to be a simple and practical approach to investigating the non-linear instability and breakup of a liquid jet. Tropey [**37**] utilized variations of Lee's numerical-simulation methodology in his analyses of the instability of inviscid liquid jets. By examining Weber's [**5**] linear instability analysis of a viscous liquid jet, Sellens [**38**] modified Lee's basic formulation to include viscous terms. He argued that viscous forces become more paramount at a smaller jet radius. Since most atomizers are of small scale, the effects of liquid viscosity should be included in numerical simulations of the atomization process to enhance their accuracy.

Swirling liquid jets have received limited attention in the literature despite their distinctive characteristics, which are absent in their non-rotating counterparts. The presence of centrifugal forces in swirling jets critically alters their stability characteristics by combining both Kelvin–Helmholtz (shear) and Taylor–Gortler (centrifugal) instabilities. The bulk of the published research in the area of swirling jet atomization makes use of the linear instability theory. Ponstein [**39**] presented a comprehensive linearized treatment of the problem. Kang and Lin [**40**] analysed the effects of non-axisymmetric disturbances on the linear instability of a swirling liquid jet surrounded by a non-swirling gas. Lian and Lin [**41**] considered the convective linear instability of a viscous liquid jet issued in a swirling inviscid gas. Wu *et al.* [**34**] investigated the spatial instability of an inviscid compound jet with swirl distribution of solid-body rotation, and free vortex in and outside the vortex core, respectively. Ibrahim [**42**] modelled the non-linear capillary instability and breakup of a swirling liquid jet by modifying Lee's equations to incorporate the additional terms needed to account for the swirl ensuing from superposing a free vortex on the mean flow. More recently, Park *et al.* [**43**] applied the boundary element method to model the non-linear instability of a swirling liquid column.

In the present work, the studies of Ibrahim [**42**] are extended by adding the effect of viscosity on liquid jet atomization to that of the swirl. Therefore, this effort emphasizes the combined influence of viscous forces investigated by Sellens [**38**], and centrifugal or swirl forces studied by Ibrahim [**42**]. In addition, the exact form of the surface tension term as given by Levich [**44**] is incorporated to replace the linearized version used by Ibrahim [**42**] and Sellens [**37**]. A novel derivation of the governing equations in conservative form is detailed. A rigorous total variation diminishing (TVD) with flux splitting and characteristic decomposition finite-difference scheme is used to ensure the accuracy and stability of the numerical simulations. Therefore, numerical instabilities reported by other investigators [**31**, **38**] in obtaining solutions of the governing equations are eliminated. These instabilities may have originated from the application of central-differencing-based finite difference schemes, particularly at smaller viscous forces. The present model also contributes an innovative methodology for taking into account swirl and viscous effects by including them in the source terms of the governing equations.

The evolution of the deformed jet surface leading to formation of main and satellite drops, commonly observed in liquid jet breakup, is simulated and examined. The size of drops produced by jet disintegration is computed. Effects of flow conditions and liquid properties on the resultant spray parameters are investigated. The present model is intended to explicate the influence of the swirl and viscosity on liquid jet atomization. The model could be used in designing spray nozzles with specific applications that may benefit from the unique features produced by liquid swirl. However, it should be pointed out that the range of Weber and Reynolds numbers investigated in the present work yields jet breakup by, primarily, the capillary forces rather than inertia. Therefore, the model would be most applicable to physical technology involving atomization of low-speed jets such as ink-jet printing, agricultural sprays, coating, and painting.

2 THEORETICAL FORMULATION

The instability of an infinitely long cylindrical liquid jet subject to an initial sinusoidal disturbance is considered. The liquid is assumed to be viscous and incompressible. The axial velocity is assumed to be constant over the cross-section of the jet and dependent only on axial coordinate z and time t. These assumptions are consistent with the study of the case of long waves [**44**]. Since the surrounding conditions and velocity distribution at each cross-section within the jet is uniform, the jet surface will be axisymmetric during the wave growth. In a cylindrical coordinate system moving at the unperturbed (basic) axial jet velocity relative to the gas, the equations of motion may be written in their conservative form as

Continuity

$$\frac{1}{r}\frac{\partial}{\partial r}(rv) + \frac{\partial}{\partial z}(u) = 0 \tag{1}$$

Downloaded from pic.sagepub.com at PENNSYLVANIA STATE UNIV on September 17, 2016

Axial momentum

$$\frac{\partial}{\partial t}(u) + \frac{1}{r}\frac{\partial}{\partial r}(rvu) + \frac{\partial}{\partial z}(uu) = -\frac{1}{\rho_\ell}\frac{\partial}{\partial z}(p) + \nu_\ell \frac{\partial^2 u}{\partial z^2} \tag{2}$$

Since the interface is a material surface, the radial velocity component is given by

$$v = \frac{\partial h}{\partial t} + \frac{\partial h}{\partial z}\frac{\partial z}{\partial t} = \frac{\partial h}{\partial t} + u\frac{\partial h}{\partial z} \tag{3}$$

By multiplying each of equations (1) and (2) by the radial coordinate, r, integrating from 0 to h, the radius of the perturbed jet, and substituting for the radial velocity component from equation (3), a set of unsteady one-dimensional equations is derived

$$\frac{\partial(h^2)}{\partial t} + \frac{\partial(h^2 u)}{\partial z} = 0 \tag{4}$$

$$\frac{\partial(h^2 u)}{\partial t} + \frac{\partial(h^2 u^2)}{\partial z} = -\frac{h^2}{\rho_\ell}\frac{\partial p}{\partial z} + \nu_\ell h^2 \frac{\partial^2 u}{\partial z^2} \tag{5}$$

It should be noted that equations (4) and (5) are identical to those derived by Sellens [**38**] except for the viscous term. Sellens [**38**] derived his equations by considering mass and axial momentum balances on a disc-shaped element of the liquid jet. Therefore, Sellens's [**38**] approach involved geometrical simplifying assumptions that are not employed in the present model, resulting in discrepancy in the form of the viscous terms between the two models.

The radial momentum equation for a symmetric liquid jet with negligible radial velocity compared to tangential velocity is reduced to

$$-\frac{w^2}{r} = -\frac{1}{\rho_\ell}\frac{\partial p}{\partial r} \tag{6}$$

Following Ponstein [**39**], a swirl (tangential) velocity, $w = A/r$, corresponding to a free vortex of constant strength A centred at the jet axis is considered. Through integration of equation (6) between the limits of any radial position r and the interfacial position h, it is shown that [**42**]

$$p_h = p - \frac{1}{2}\rho_\ell A^2\left(\frac{1}{h^2} - \frac{1}{r^2}\right) \tag{7}$$

The normal stresses due to liquid pressure, viscous stresses, gas pressure, and surface tension are balanced at the liquid–gas interface, $r = h$, therefore

$$-p_h + 2\mu_\ell \frac{\partial v}{\partial r} + p_\sigma = -p_{\mathrm{g}} \tag{8}$$

Substitution from equation (7) into equation (8) yields

$$p = \frac{1}{2}\rho_\ell A^2\left(\frac{1}{h^2} - \frac{1}{r^2}\right) + p_\sigma + p_{\mathrm{g}} \tag{9}$$

It should be noted that the viscous term in equation (8) vanishes by virtue of equation (3) and the assumption that velocity is independent of radial distance. The capillary pressure is derived by Levich [**44**] as

$$p_\sigma = \frac{\sigma}{h}\left\{\frac{1}{\sqrt{1 + (\partial h/\partial z)^2}} - \frac{h(\partial^2 h/\partial z^2)}{\sqrt{[1 + (\partial h/\partial z)^2]^3}}\right\} \tag{10}$$

Substituting equation (10) in equation (9) after ignoring gas pressure perturbations, carrying out the differentiation of the pressure term with respect to z, and rewriting both equations (4) and (5) in dimensionless form, the following can be obtained

$$\frac{\partial H^2}{\partial T} + \frac{\partial(H^2 U)}{\partial Z} = \mathbf{S}(1,1) \tag{11}$$

$$\frac{\partial(H^2 U)}{\partial T} + \frac{\partial(H^2 U^2)}{\partial Z} = \mathbf{S}(2,1) \tag{12}$$

where $\mathbf{S}$ is the source matrix with two elements, namely, $\mathbf{S}(1,1) = 0$, and $\mathbf{S}(2,1)$ given by

$$\mathbf{S}(2,1) = \frac{We_{\mathrm{s}}}{H}\frac{\partial H}{\partial Z} + \left\{\frac{\partial H/\partial Z}{\sqrt{1 + (\partial H/\partial Z)^2}} + \frac{H(\partial H/\partial Z)(\partial^2 H/\partial Z^2) + H^2(\partial^3 H/\partial Z^3)}{\sqrt{[1 + (\partial H/\partial Z)^2]^3}} - \frac{3H^2(\partial H/\partial Z)(\partial^2 H/\partial Z^2)^2}{\sqrt{[1 + (\partial H/\partial Z)^2]^5}}\right\} + \frac{H^2}{Re_\sigma}\frac{\partial^2 U}{\partial Z^2} \tag{13}$$

All lengths are normalized by the jet radius, a, velocity is non-dimensionalized by the capillary velocity, $U_\sigma = \sqrt{\sigma/\rho_\ell a}$, and time is made dimensionless by multiplying by the capillary velocity and dividing by the jet radius. The terms on the right-hand side of equation (13) correspond to swirl, capillary, and viscous forces, respectively. The treatment of the swirl, capillary, and viscous terms as source terms is to avoid the numerical instability that may originate from these terms, as was documented by previous investigators [**31**, **38**].

The initial conditions correspond to a sinusoidal disturbance imposed on the unperturbed interface, so that

$$H(t = 0, z) = \eta_0 \cos(KZ) + 1 \tag{14}$$

$$U(t = 0, z) = 0 \tag{15}$$

where η_0 is the amplitude of initial disturbance. Since it is not practical to simulate the whole length of the jet, the computational domain is taken to be equal to one wavelength $\lambda = 2\pi/k$ and a symmetric boundary condition is applied at the right and left ends of this domain.

Downloaded from pic.sagepub.com at PENNSYLVANIA STATE UNIV on September 17, 2016

The dimensionless continuity and axial momentum equations given by equations (11) and (12), may be written in matrix form as

$$\frac{\partial \mathbf{E}}{\partial T} + \frac{\partial \mathbf{F}}{\partial Z} = \mathrm{S} \tag{16}$$

where

$$\mathbf{E} = \begin{bmatrix} H^2 \\ H^2 U \end{bmatrix} \tag{17}$$

$$\mathbf{F} = \begin{bmatrix} H^2 U \\ H^2 U^2 \end{bmatrix} \tag{18}$$

The present numerical simulations employ a TVD scheme with flux-splitting and characteristic decomposition to obtain solutions of the system of equations given by equation (16). The TVD upwind method uses two characteristic speeds of the convective eigen vector to determine the upwind direction. Therefore, the flux term can be calculated with the following formula

$$\mathbf{F}_{i-1/2} = \frac{1}{2}(\mathbf{F}_i + \mathbf{F}_{i-1}) - \frac{1}{2}|\boldsymbol{G}|(\mathbf{E}_i - \mathbf{E}_{i-1}) \tag{19}$$

where $\boldsymbol{G}$ is the eigen vector of the system. Accordingly, the finite-difference solutions of the dependent variables in the matrix $\mathbf{E}$ over the control volume can be obtained through

$$\mathbf{E}_i^{m+1} = \mathbf{E}_i^m - \frac{\Delta T}{\Delta Z}(\mathbf{F}_{i+1/2}^m - \mathbf{F}_{i-1/2}^m) + \Delta T \mathbf{S}_i^m \tag{20}$$

For the present computations, the time step was set as 1 per cent of the spatial step size. The computational domain was equal to one wave length and a uniform mesh system was used. The number of nodes for the one-dimensional grid was chosen as 20, which rendered a grid-independent convergent numerical solution.

3 RESULTS AND DISCUSSION

In the present computations, the liquid and gas properties are taken as those of water injected into atmospheric air. The initial jet radius is taken as 0.0005 m. The dimensionless parameters, e.g. the Weber number and Reynolds number, are therefore determined based on these fluid properties and relevant flow parameters.

The time-history of the disturbance growth rate may be indicative of the convergence of the numerical solutions. Therefore, the temporal variation of the dimensionless growth rate is scrutinized in Fig. 1 for the dimensionless wave number, $K = 1.0$, that corresponds to the maximum growth rate for $We_s = 1.0$, as expounded in Fig. 2. The capillary Reynolds number, based on water properties and an initial jet radius of

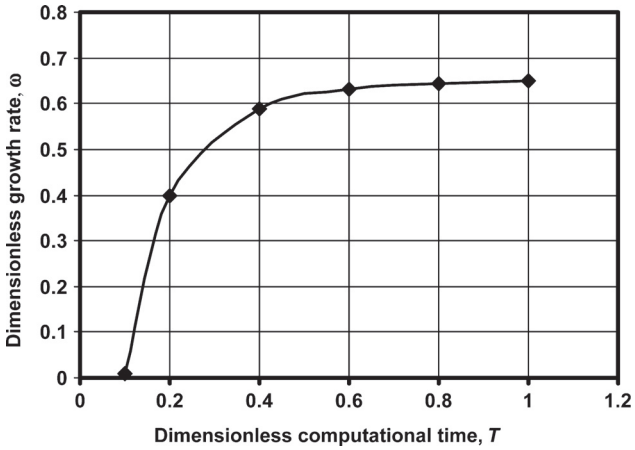

Fig. 1 Time-history of dimensionless disturbance growth rate

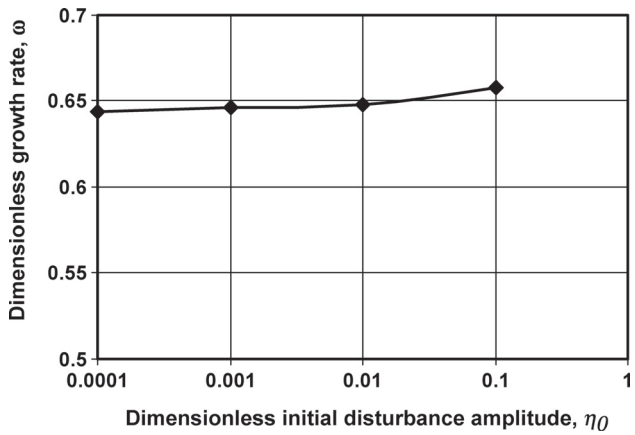

Fig. 2 Variation of growth rate with initial displacement amplitude

$a = 0.0005$ m, is approximately $Re_\sigma = 200$. The dimensionless growth rate plotted in Fig. 1 is calculated at each time step by the numerical method suggested by Mansour and Lundgren [**32**]

$$\omega = \frac{\Delta H / \Delta T}{\sqrt{(H-1)^2 - \eta_0^2}} \tag{21}$$

The growth rate is determined by averaging the overall spatial discretization nodes of the numerical solution. The value of η_0 used in eqution (21) is taken as, $\eta_0 = 0.01$ as discussed in the following paragraph. It is seen in Fig. 1 that the growth rate history exhibits an initial interval of rapid increase followed by a fairly asymptotic behaviour that is indicative of a stable solution. Therefore, the growth rate in the present work is deemed to be represented by its asymptotic value at the jet breakup instant.

The initial disturbance amplitude used in the computations may have an effect on the growth rate of

Downloaded from pic.sagepub.com at PENNSYLVANIA STATE UNIV on September 17, 2016

disturbances. It is desirable to keep the initial disturbance amplitude small to observe the initial stages of the evolution of disturbances on the liquid jet surface and minimize numerical instability. However, employing relatively small initial disturbance amplitude results in an unnecessary long computational time. To decide upon an acceptable level of the initial amplitude of disturbance, its influence on disturbance growth rate is examined in Fig. 2 at the same conditions of Fig. 1, i.e. $K = 1.0$, $We_s = 1.0$, and $Re_\sigma = 200$. It is observed in Fig. 3 that the dimensionless initial amplitude does not have much effect on the dimensionless growth rate when $\eta_0 \leqslant 0.01$. Therefore, the amplitude of the initial disturbance is set at 1 per cent of the unperturbed jet radius throughout this study.

To further validate the model, comparison of computational predictions with published theoretical analyses are performed. Ponstein [**39**] advanced a linear stability analysis of a swirling inviscid liquid jet subjected to a basic potential flow having a constant axial velocity and a tangential (swirl) velocity of the form A/r, which corresponds to a free vortex centred at the jet axis. For axisymmetric disturbances, Ponstein gives the dimensionless growth rate as

$$\omega = \sqrt{(We_s + 1 - K^2)\frac{I_1(K)}{I_0(K)}K} \tag{22}$$

where the growth rate is made dimensionless by dividing by $\sqrt{\sigma/(\rho a^3)}$, and I_0 and I_1 are the modified Bessel functions of the first kind of zero and first order, respectively.

Figure 3 depicts the comparison of the present nonlinear model's dimensionless disturbance growth rate computations with Pontstein's [**39**] theoretical results. The disturbance dimensionless growth rate is plotted in Fig. 3 as a function of the dimensionless wave number at a capillary Reynolds number, $Re_\sigma = 200$, and swirl Weber numbers, $We_s = 0$, 1, and 2. It is clear from Fig. 3 that the numerical simulations agree well with Ponstein's analysis, thus affirming confidence in the computational model's robustness. However, the non-linear predictions yield growth rates somewhat lower than those produced by the linear theory, especially at higher swirl Weber numbers. Similar trends also have been described by Childs and Mansour [**45**] for the non-swirling jet, and Ibrahim [**42**] in the case of inviscid swirling jet. The drop in the predicted growth rate relative to that of Ponstein's may be explained by the dual dampening effects of non-linearity and viscosity included in the present model. These effects combine to reduce the disturbance growth below its exponential rate assumed in the linear inviscid theory of Ponstein [**39**]. Figure 3 also indicates that increasing swirl leads to a more pronounced disturbance growth rate and larger cut-off wave number, i.e. the range of the wave number for which jet instability is realized. It is also seen in Fig. 3 that the dominant wave number, which corresponds to maximum growth rate, becomes larger as swirl Weber number is increased. Since a larger wave number is associated with a shorter disturbance wavelength, increasing swirl strength may lead to formation of smaller drops.

The effects of the swirl and viscosity on the evolution of interfacial disturbances on the liquid jet surface are investigated in Figs 4, 5, 6, and 7. Results for the non-swirling jet corresponding to $We_s = 0.0$ are displayed in Fig. 4 at capillary Reynolds number, $Re_\sigma = 200$, and the dimensionless dominant wave number corresponding to maximum growth for the non-swirling jet, $K = 0.7$. It should be indicated that the interfacial contour lines in Figs 4, 5, 6, and 7 are separated by 100 time steps. Recall that the dimensionless time step

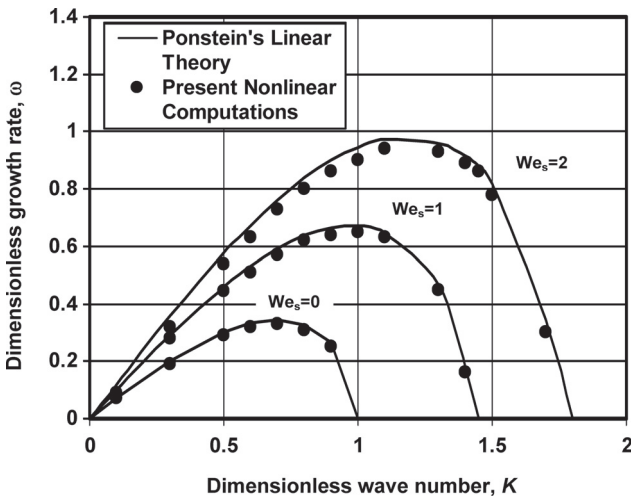

Fig. 3 Comparison of present non-linear computations with linear theory

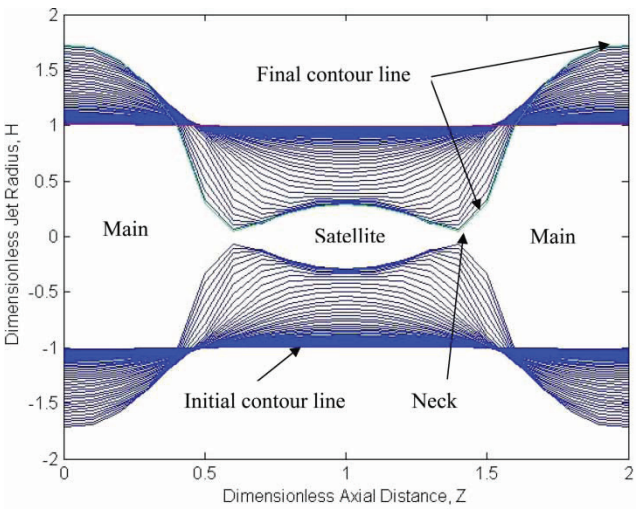

Fig. 4 Evolution of liquid jet interface at $K = 0.7$, $We_s = 0$, and $Re_\sigma = 200$

Downloaded from pic.sagepub.com at PENNSYLVANIA STATE UNIV on September 17, 2016

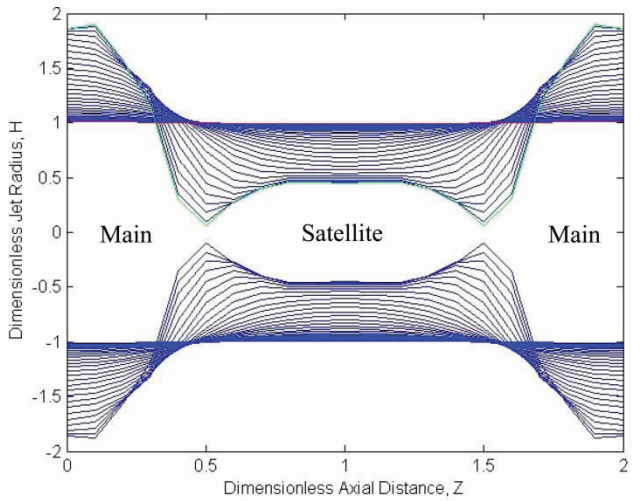

Fig. 5 Evolution of liquid jet interface at $K = 0.7$, $We_s = 1.0$, and $Re_\sigma = 200$

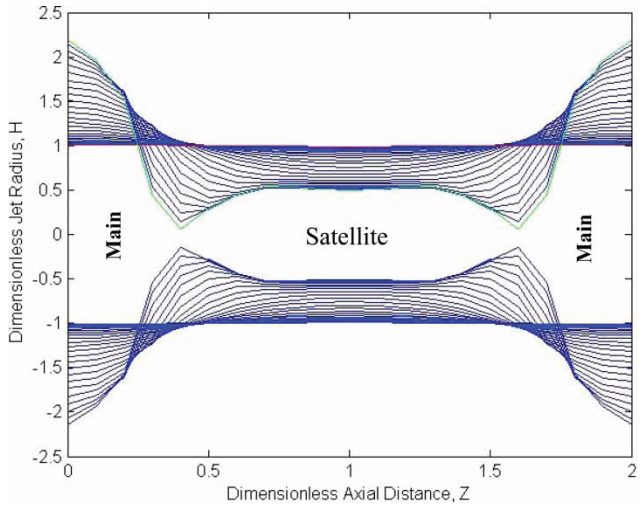

Fig. 6 Evolution of liquid jet interface at $K = 0.7$, $We_s = 2.0$, and $Re_\sigma = 200$

is set at $\Delta T = 0.01$ $\Delta Z = 0.01$ $(\lambda/an) = 0.01$ $(2\pi/Kn)$, where n is the number of grid points taken as 20. Since the total dimensional domain investigated is one wave length, $\lambda = 2\pi/K$, the dimensionless axial distance is normalized by K/π, so that it varies from 0 to 2.0. The dimensionless time of interfacial evolution may be calculated by multiplying the number of contour lines between the initial and final states of the interface by $100\Delta T$.

Figure 4 illustrates the spatial growth of the infinitesimal initial disturbances to a finite size. The contour lines in Fig. 4, which are plotted 100 time steps apart, follow the progress of the liquid jet interface from an initially undisturbed cylindrical shape through its development in time. It is noted in Fig. 4 that the jet surface distortion leads to

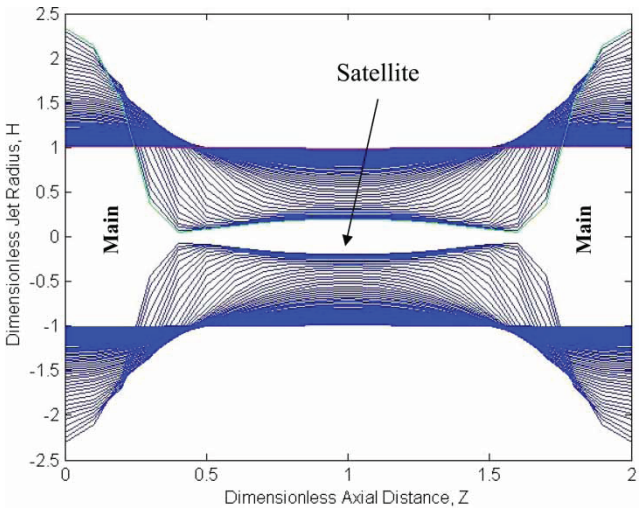

Fig. 7 Evolution of liquid jet interface at $K = 0.7$, $We_s = 0$, and $Re_\sigma = 2$

formation of large main drops with smaller satellite drops interspaced between them, as has been recognized in past studies [**16–26**, **31–33**, **35–38**]. When the necking portion of the jet touches the centreline, i.e. $H = 0$, the main and satellite drops will detach from the jet. Since this condition may lead to a singularity in the numerical solution, the criterion adopted to stop the computations was that $H \leqslant 0.05$ at any nodal point on the interface. Using this criterion, the drop radii can be estimated. The boundary between main and satellite drops was set at the location on the jet interface that is closest to the centreline. Since the drops were mostly far from spherical, a composite trapezoidal rule was used to integrate the breakup volume of drops, and hence the equivalent radius of a sphere of the same volume can be determined.

Figures 5 and 6 portray, respectively, the effects of introducing the swirl of $We_s = 1.0$, 2.0 into the liquid jet, on the development of interfacial disturbances. All the other problem parameters investigated in Figs 5 and 6 are held the same as in Fig. 4. It is evident from the progressive decrease in the number of interfacial lines in Figs 5 and 6 compared with Fig. 4 that the liquid swirl promotes the growth of instability waves on the jet surface (recall that each line represents $100\,\Delta T$). This higher growth rate maybe attributed to the additional pressure gradient created in the liquid due to the swirl. Therefore, swirling the liquid jet will cause it to break up at a faster rate, and hence enhance its atomization. This result is in general agreement with previous work [**39**, **40**, **42**, **43**].

It is also seen from Figs 4, 5, and 6 that increasing swirl causes the main drops to deviate from sphericity and assume a donut-like shape, while the satellite drops take a more elongated oval shape.

Downloaded from pic.sagepub.com at PENNSYLVANIA STATE UNIV on September 17, 2016

In order to investigate the effect of liquid viscosity on the development of jet disturbance, all parameters are kept the same as those in relation to Fig. 4, except that the Reynolds number is reduced to $Re_\sigma = 2$, signifying a two order of magnitude rise in liquid kinematic viscosity over that considered in Fig. 4. The results of Fig. 7 elucidate that increasing liquid viscosity by 100-fold results in an appreciable stretching of the main drops in the radial direction, leading them to resemble a disc shape. The satellite drops experience a significant axial elongation. It is also clear from Fig. 7 that the time elapsed for the interface to approach the breakup criterion has increased by about 20 per cent, as evident from the larger number of interfacial lines appearing in Fig. 7 compared with Fig. 4. This result is expected due to the dissipative nature of liquid viscosity that leads to suppression of the growth of surface waves. Therefore, it is concluded that the effects of variation in the viscous term exhibit a plausible trend.

Figure 8 portrays the variation of dimensionless main and satellite drop radii with wave numbers at capillary Reynolds number, $Re_\sigma = 200$, and swirl Weber numbers, $We_s = 0$, 1, and 2. It is remarked in Fig. 8 that the size of both main and satellite drops decrease with wave number. This is expected since the disturbance wavelength becomes smaller as the wave number is increased, and hence the volume of liquid available to produce individual main and satellite drops is reduced. It is also noticed that, for all swirl values investigated, the size of main and satellite drops approach each other at small wave numbers, i.e. long wave lengths. A similar trend has been reported in relation with the Rayleigh jet [**19**, **31**].

It is also observed in Fig. 8 that, at the same wave number, the size of the main drops is reduced while that of the satellite drops is augmented as the swirl Weber number is raised. This behaviour is a consequence of centrifugal forces acting to displace liquid mass from the larger main drops to smaller satellite ones.

Figure 9 elucidates the variation of dimensionless main and satellite drop radii with swirl Weber numbers at the dimensionless wave number, $K = 1.0$, and capillary Reynolds number, $Re_\sigma = 200$. For each value of swirl Weber number, the computations are performed at the dominant wave number corresponding to the maximum growth rate as determined from the linear theory of Ponstein [**39**]. It is seen in Fig. 9 that increasing the swirl strength causes the size of both main and satellite drops to be diminished. This is due to the rise in the dominant wave number and hence reduction of wavelength with the swirl Weber number, as discussed earlier in relation to Fig. 3. It is manifested in Fig. 9 that for a change of the swirl Weber number from 0 to 2, the sizes of both main and satellite drops are reduced by approximately 25 per cent of their original size.

Figure 10 delineates the variation of dimensionless main and satellite drop radii with capillary Reynolds numbers at the dimensionless wave number, $K = 1.0$,

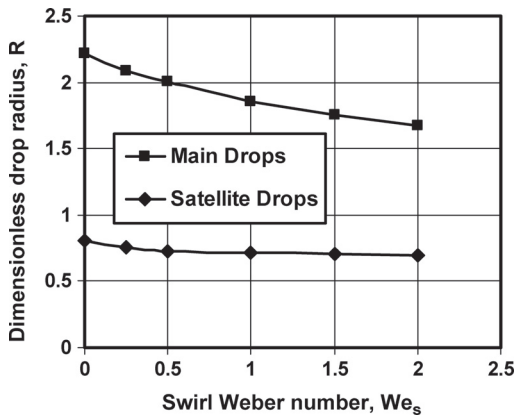

Fig. 9 Effect of swirl on drop size

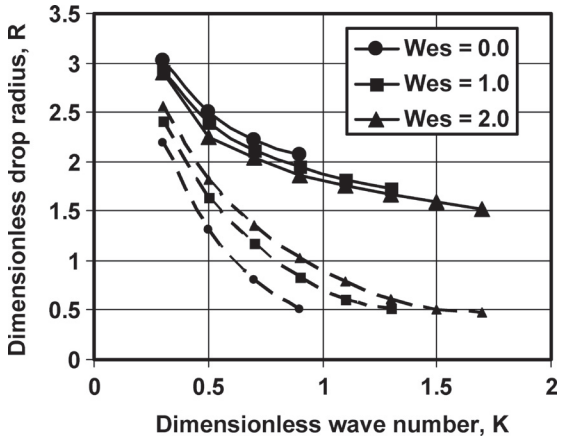

Fig. 8 Variation of drop size with wave number

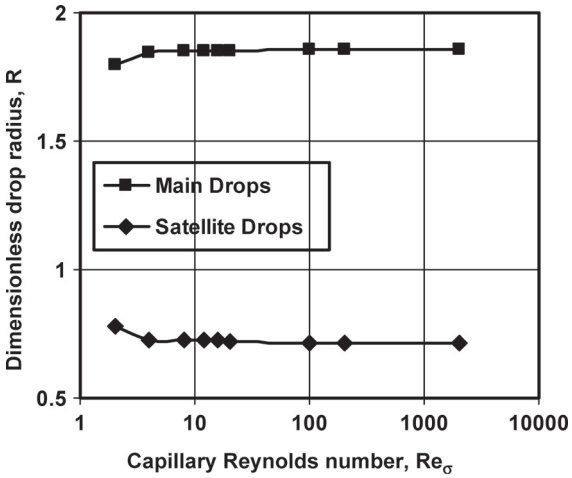

Fig. 10 Effect of viscosity on drop diameter

Downloaded from pic.sagepub.com at PENNSYLVANIA STATE UNIV on September 17, 2016

and swirl Weber number, $We_s = 1$. It is deduced from Fig. 10 that for small Reynolds numbers up to $Re_\sigma = 100$, the size of main drops increase while that of the satellite drops decrease as the capillary Reynolds number is increased. For the range of capillary Reynolds number from 2 to 100, the size of main drops grows by about 4 per cent of its original size while that of satellite drops experiences a reduction of ≈12 per cent. This behaviour may be interpreted in the light of the enhanced viscous dissipation effects at smaller Reynolds numbers, which act to inhibit development of the bigger main drops and thus leaves more liquid volume available for smaller satellite drops to consume. Figure 10 also demonstrates that increasing the capillary Reynolds number above $Re_\sigma = 100$ has no effect on drop sizes, indicating that liquid viscosity has become too small to affect drop formation.

4 CONCLUSIONS

A rigorous mathematical formulation and numerical solution scheme of the computational model equations for a swirling viscous liquid jet are demonstrated.

The model affords a simple method to account for the swirl and viscous effects through inclusion in the source terms of the governing equations. The swirl is represented by a free vortex introduced in the normal stress boundary condition. The computational model appropriately captures the influence of the swirl and viscous forces on the instability and breakup of the liquid jet. Validation of the model against established theoretical results reveal good agreement. A larger swirl Weber number boosts jet destabilization due to a more pronounced pressure differential across the jet cross-section. Decreasing the capillary Reynolds number causes the instability of the liquid jet to be hampered by the dampening effects of viscosity. Respective radial and axial distortions of the shapes of main and satellite drops are brought about by the swirl and viscous forces. Increasing the disturbance wave number yields smaller main and satellite drops. A larger swirl Weber number is associated with an enlarged dominant wave number, and hence a reduced size of main and satellite drops. For capillary Reynolds numbers less than 100, increasing liquid viscosity leads to augmentation of satellite drops size at the expense of that of the main drops.

ACKNOWLEDGEMENTS

This work has been supported by NASA under Constellation University Institute Project (CUIP), Rocket Engine Advancement Program (REAP) under contracts #NNM05AA22A, NNC06GA29G, and NCC3-994.

REFERENCES

1 **Rayleigh, J. S.** and **Lord, W.** On the instability of jets. *Proc. Lond. Math. Soc.*, 1878, **10**, 4–13; also in, Rayleigh, Lord, *Scientific papers*, vol. 1, 1899, p. 361 (Cambridge University Press, Cambridge); see also *The theory of sound*, 2nd edition, vol. 2, 1896 (MacMillan, London) 1945, pp. 351, 360–376, 366, 504 (reprinted by Dover Publications, Inc., New York).
2 **Rayleigh, J. S.** and **Lord, W.** On the capillary phenomena of jets. *Proc. R. Soc. Lond.*, 1879, **29**, 71–97.
3 **Rayleigh, J. S.** and **Lord, W.** Further observations upon liquid jets. *Proc. R. Soc. Lond.*, 1882, **34**, 130–145.
4 **Rayleigh, J. S.** and **Lord, W.** On the stability of a cylinder of viscous liquid under capillary forces. *Philosophical magazine*, vol. 34, 1892, p. 145; also in Rayleigh, Lord, *Scientific papers*, vol. 3, 1902, pp. 585–593 (Cambridge University Press, Cambridge).
5 **Weber, C.** On the breakdown of a fluid jet. *Z. Agnew. Math. Mech.*, 1931, **11**, 138–145.
6 **Tomotika, S.** On the instability of a cylindrical thread of a viscous liquid surrounded by another viscous fluid. *Proc. R. Soc. Lond.*, 1935, **150**(A), 322–337.
7 **Sterling, A. M.** and **Sleicher, C. A.** Stability of capillary jets. *J. Fluid Mech.*, 1975, **68**, 477–495.
8 **Reitz, R. D.** and **Bracco, F. V.** Mechanism of atomization of liquid jets. *Phys. Fluids*, 1982, **25**, 1730–1742.
9 **Lin, S. P.** and **Lian, Z. W.** Mechanism of the breakup of liquid jets. *AIAA J.*, 1990, **28**(1), 120–126.
10 **Lin, S. P.** and **Ibrahim, E. A.** Instability of a viscous liquid jet surrounded by a viscous gas in a vertical pipe. *J. Fluid Mech.*, 1990, **218**, 641–658.
11 **Grant, R. P.** and **Middleman, S.** Newtonian jet stability. *AICHE J.*, 1966, **12**(4), 669–678.
12 **McCarthy, M. J.** and **Molloy, N. A.** Review of stability of liquid jets and the influence of nozzle design. *Chem. Eng. J.*, 1974, **7**, 1–20.
13 **Mahoney, T. J.** and **Sterling, M. A.** The breakup length of laminar newtonian liquid jets in air. In Proceedings of the 1st International Conference on Liquid Atomization and Spray Systems, Tokyo, 1978, pp. 9–12.
14 **Wang, D. P.** Finite amplitude effect on the stability of a jet of circular cross-section. *J. Fluid Mech.*, 1968, **4**(2), 299–313.
15 **Yuen, M. C.** Non-linear capillary instability of a liquid jet. *J. Fluid Mech.*, 1968, **33**(1), 151–163.
16 **Nayfeh, A. H.** Non-linear stability of a liquid jet. *Phys. Fluids*, 1970, **13**(4), 841–847.
17 **Nayfeh, A. H.** and **Hassan, S. D.** The method of multiple scales and non-linear dispersive waves. *J. Fluid Mech.*, 1971, **49**, 463.
18 **Kakutani, T., Inoue, Y.,** and **Kan, T.** Non-linear capillary waves on the surface of liquid column. *J. Phys. Soc. Jpn.*, 1974, **37**, 529–538.
19 **Lafrance, P.** Non-linear breakup of a liquid jet. *Phys. Fluids*, 1975, **18**(4), 428–432.
20 **Taub, H. H.** Investigation of non-linear waves on liquid jets. *Phys. Fluids*, 1976, **19**, 1124–1129.
21 **Chaudhary, K. C.** and **Redekopp, L. C.** The non-linear capillary instability of a liquid jet, part 1: theory. *J. Fluid Mech.*, 1980, **96**(2), 257–274.

Downloaded from pic.sagepub.com at PENNSYLVANIA STATE UNIV on September 17, 2016

22 Bogy, D. B. Use of a one-dimensional cosserat theory to study instability in a viscous liquid jet. *Phys. Fluids*, 1978, **21**, 190–197.

23 Bogy, D. B. Wave propagation and instability of a circular semi-infinite liquid jet harmonically forced at the nozzle.*Trans. ASME, J. Appl. Mech.*, 1978, **45**, 469–474.

24 Bogy, D. B. Breakup of a liquid jet: second perturbation solution for one-dimensional cosserat theory. *IBM J. Res. Dev.*, 1979, **23**, 87–91.

25 Bogy, D. B. Breakup of a liquid jet: third perturbation cosserat solution. *Phys. Fluids*, 1979, **22**(2), 224–230.

26 Bogy, D. B. Drop formation in a circular liquid jet. *Annu. Rev. Fluid Mech.*, 1979, **11**, 207–228.

27 Green, A. E. and **Naghdi, P. M.** On the theory of rods II: developments by direct approach. *Proc. R. Soc. Lond. A*, 1974, **337**, 485–507.

28 Green, A. E. On the non-linear behavior of fluid jets. *Int. J. Eng. Sci.*, 1976, **14**(1), 49–63.

29 Ibrahim, E. A. and **Lin, S. P.** Weakly non-linear instability of a liquid jet in a viscous gas. *Trans. ASME, J. Appl. Mech.*, 1992, **59**(2), S291–S296.

30 Fromm, J. E. Numerical calculation of the fluid dynamics of drop-on-demand. *IBM J. Res. Dev.*, 1984, **28**, 322–333.

31 Shokoohi F. and **Elrod, H. G.** Numerical investigation of the disintegration of liquid jets. *J. Comput. Phys.*, 1987, **71**(2), 324–342.

32 Mansour, N. N. and **Lundgren, T. S.** Satellite formation in capillary jet breakup. *Phys. Fluids A*, 1990, **2**(7), 1141–1144.

33 Chacha, M., Radev, S., Tadrist, L., and **Occelli, R.** Numerical treatment of the instability and the breakup of a liquid capillary column in a bounded immiscible phase. *Int. J. Multiph. Flow*, 1997, **23**(2), 377–395.

34 Wu, C., Farokhi, S., and **Taghavi, R.** Spatial instability of a swirling jet – theory and experiment. *AIAA J.*, 1992, **30**(6), 1545–1552.

35 Lee, H. C. Drop formation in a liquid jet. *IBM J. Res. Dev.*, 1974, **18**, 364–369.

36 Pimbley, W. T. and **Lee, H. C.** Satellite droplet formation in a liquid jet. *IBM J. Res. Dev.*, 1977, **21**, 21–30.

37 Tropey, P. A. A non-linear theory for describing the propagation of disturbances on a capillary jet. *Phys. Fluids A*, 1989, **1**, 661–667.

38 Sellens, R. W. A one-dimensional numerical model of capillary instability. *Atomization Sprays*, 1992, **2**(3), 239–251.

39 Ponstein, J. Instability of rotating cylindrical jets. *Appl. Sci. Res.*, 1959, **8**(A), 425–456.

40 Kang, D. J. and **Lin, S. P.** Breakup of a swirling liquid jet. *Int. J. Eng. Fluid Mech.*, 1989, **2**(1), 47–62.

41 Lian, Z. W. and **Lin, S. P.** Breakup of a liquid jet in a swirling gas. *Phys. Fluids A*, 1990, **2**(12), 2134–2139.

42 Ibrahim, E. A. Effect of swirl on jet atomization. *AIAA J.*, 1993, **31**(12), 2376–2377.

43 Park, H., Yoon, S. S., and **Heister, S. D.** On the non-linear stability of a swirling liquid jet. *Int. J. Multiph. Flow*, 2006, **32**(9), 1100–1109.

44 Levich, V. G. *Physicochemical hydrodynamics*, 1962, p. 635 (Prentice Hall, Upper Saddle River, New Jersey).

45 Childs, R. E. and **Mansour, N. N.** Simulation of fundamental atomization mechanisms in fuel spray. *J. Propuls.*, 1989, **5**(6), 641–649.

APPENDIX

Notation

a	unperturbed liquid jet radius
A	free vortex strength
$\boldsymbol{G}$	eigen vector
h	perturbed liquid jet radius
H	dimensionless perturbed liquid jet radius, $H = h/a$
k	wave number
K	dimensionless wave number, $K = ka$
p	perturbation pressure
r	radial coordinate
R	dimensionless drop radius
Re_σ	liquid Reynolds number based on capillary velocity, $Re_\sigma = U_\sigma a/\nu_\ell$
$\mathbf{S}$	source matrix
t	time
T	dimensionless time, $T = t(U_\sigma/a)$
u	liquid jet axial velocity perturbation
U	dimensionless liquid jet axial velocity, $U = u/U_\sigma$
U_σ	capillary velocity, $U_\sigma = \sqrt{\sigma/(\rho_\ell a)}$
v	liquid jet radial velocity perturbation
w	liquid jet tangential (swirl) velocity
We_s	swirl Weber number, $We_s = \rho_\ell A^2/(\sigma a)$
z	axial coordinate
Z	dimensionless axial coordinate, $Z = z/a$
Δ	step size
η	dimensionless amplitude of disturbance
λ	wave length, $\lambda = 2\pi/k$
μ	dynamic viscosity
ν	kinematic viscosity
ρ	density
σ	surface tension
ω	dimensionless growth rate of disturbance

Superscript and subscripts

m	index of time marching
0	initial (unperturbed)
g	gas
h	liquid jet interface
i	index of ith grid
ℓ	liquid
s	swirl
σ	surface tension (capillary forces)

Downloaded from pic.sagepub.com at PENNSYLVANIA STATE UNIV on September 17, 2016